JTTEE5 4:153-162

One-Dimensional Mathematical Model for Selecting Plasma Spray Process Parameters

S. Das, V.K. Suri, U. Chandra, and K. Sampath

A simple, unified, one-dimensional model has been developed to relate the effects of plasma spray parameters on the temperature and velocity of the plasma and particles and on the void content in the coating. The torch, spray, and substrate regions in a plasma spray process were first modeled independently and then coupled so that the plasma and particle characteristics calculated in one region served as inputs for the subsequent region. Comparison of the model predictions with experimental data showed reasonable agreement. Deviations from the measured data were attributable to the simplifying assumptions used in modeling the different regions of the process. A parametric analysis of the unified one-dimensional model showed that, despite its simplicity, the model is well suited for optimizing process parameters in terms of particle type and size to obtain high-integrity coatings.

1. Introduction

THE quality of plasma spray coatings primarily depends on feedstock (powder) characteristics and spray conditions. The spray conditions themselves are dependent on a large number of process parameters, and variations in these process parameters affect the quality of the resultant plasma spray coating (Ref 1). Additionally, several complex interactions that occur among plasma spray process parameters preclude the use of a simplified method to select or optimize a set of plasma spray conditions to obtain high-quality coatings. For example, although high particle temperature is known to produce good bond strength, it also results in high residual stresses.

Experimental and analytical research conducted over the past three decades (Ref 2-4) shows that knowledge of both the heat content of the system and the velocities of the plasma and particles is essential to control several process parameters and thus obtain high-integrity plasma spray coatings. In this respect, mathematical process models offer a cost-effective and highly flexible means for analyzing the effects of spray process parameters and generating quantitative relationships between input parameters and metallurgical characteristics that control coating quality. The models, which range from simple "closed-form" methods to highly rigorous, computer-intensive numerical schemes, enable one to gain insight into the process and thereby optimize plasma spray conditions to produce coatings of acceptable quality and with desired properties.

For the purpose of modeling, the plasma spray process is often divided into three distinct regions: the torch, the spray, and the substrate. The governing equations for mass, momentum, and energy conservation are solved in each of these regions to obtain the properties of the plasma, the particles, and the coating. Indeed, a number of assumptions are made to simplify the mathematical representations of complex physical-chemical phenomena occurring in these regions. Some of the most com-

Keywords: modeling, particle temperature, particle velocity, plasma spray process, porosity prediction

S. Das (presently at University of Detroit Mercy, Detroit, MI 48219-0900, USA), **V.K. Suri, U. Chandra,** and **K. Sampath,** Concurrent Technologies Corporation, Johnstown, PA 15904, USA

Nomenclature

A	Area of cross section
c_p	Specific heat
C_D	Drag coefficient
d	Diameter
E	Arc voltage
H	Enthalpy
H_e	Heat of evaporation of electrode
h	Heat-transfer coefficient
I	Arc current
k	Thermal conductivity
k_2	Constant in Eq 16
$\dot{m}$	Mass flow rate
$\dot{m}_e$	Mass loss rate of electrode
$\dot{m}_p$	Particle deposition rate
Nu	Nusselt number
P	Pressure
Pr	Prandtl number
$\dot{Q}$	Heat flow rate
$\dot{Q}_r$	Rate of radiant heat loss
r	Radius
Re	Reynolds number
t	Time
T	Temperature
U	Velocity
x	Axial distance
X	Coating thickness
V	Void volume
Z_p	Particle injection port distance from torch tip
Γ	Ratio of specific heats (c_p/c_v of air)
ρ	Density

Subscripts

a	Ambient
c	Coolant
p	Particle
g	Gas
s	Surface
in	Inlet
out	Outlet
i	Initial
n	Nozzle
1,2	Spray conditions

monly used assumptions include: local thermodynamic equilibrium (LTE) in the torch, symmetry of flow and temperature fields, inviscid flow of gas, uniform gas flow and temperature field undisturbed by injected particles, spherical particles of uniform size, and continuity of mass and momentum transfer.

Despite these assumptions, past efforts to model the torch, spray, and substrate regions of the plasma spray process have provided significant insight into several interacting phenomena that occur in each of these regions. The knowledge provided by these isolated models can be used to improve equipment design and operational controls.

2. Objectives

The objectives of the present work were to (1) combine several currently available analytical and numerical methods that relate the effects of process parameters with the physical phenomena occurring in all three regions into a simple, unified, one-dimensional model, and (2) utilize this unified model to provide quick estimates of process parameters and their effects on selected process and coating characteristics. Specifically, this work was aimed at providing a basic engineering tool to plasma spray process users who are primarily interested in the selection and control of process parameters to obtain high-quality coatings.

3. Background

Pfender (Ref 5), Apelian (Ref 6), Szekely and Westhoff (Ref 7), and Boulos (Ref 8) have provided phenomenological reviews of the transport phenomena occurring in the plasma spray process. These reviews cite a number of useful advances that have been made in modeling the torch region. Modeling the arc column itself was studied early by Pfender (Ref 5), Stine and Watson (Ref 9), Watson and Pegot (Ref 10), and Mazza (Ref 11). Several assumptions were made by these researchers with regard to the electromagnetic phenomena and the pattern of heat generation in the plasma torch. While many of these efforts treated the flow dynamics in the torch region as essentially laminar, Dilwari and Szekely (Ref 12) made significant progress in modeling the turbulence in gas flow. Scott et al. (Ref 13) made further improvements in modeling the magneto-fluid-dynamic phenomenon within the torch.

Several of the numerical efforts cited above are quite rigorous and use finite-difference or finite-element techniques to describe plasma torch events in two- and three-dimensional models. In simplifying the modeling effort, several researchers have utilized one-dimensional closed-form solutions (Ref 14-16). In these latter approaches, the torch region is often assumed to be isentropic with LTE conditions. The approximations to the transport phenomena are similar to those used to study supersonic gas flows. Bernoulli's law for compressible flow of gases is commonly employed to compute the velocity and temperature of the plasma and particles at the torch nozzle exit. The simplest approach, however, approximates the temperature of the plasma and particles issuing from the torch nozzle exit through empirical expressions derived from experimental data (Ref 3, 17, 18).

A number of one-, two-, and three-dimensional mathematical models have also been developed to estimate the transport of fluid and particles in the spray region. Szekely and coworkers (Ref 19, 20) utilized two-dimensional axisymmetric Navier-Stokes and energy equations to compute fluid flow and thermal characteristics of plasma spray, and addressed various issues related to plasma-particle interactions. Attempts have also been made to estimate turbulence (Ref 21) and noncontinuum effects and swirl in the spray (Ref 22, 23) in terms of their influence on particle velocities. In addition to these comprehensive methods, a number of simple yet useful analytical models have been developed to represent plasma-particle interactions. Scott and Cannell (Ref 18) used experimental data to develop analytical expressions for temperature and velocity of both the plasma and the particles. Shaw and German (Ref 24) and Vardelle et al. (Ref 3, 25) used generally similar approaches in explicitly tracking the particle path and velocity by solving one-dimensional momentum transport between the plasma and the particle, and treated the spray particles as a lumped mass to calculate the temperature rise of the particles. Joshi and Sivakumar (Ref 26) and Das and Sivakumar (Ref 27, 28) further modified the model by including the temperature variation along the droplet radius. Several of these models compared numerical estimates of plasma temperature, plasma velocity, and particle velocity with the experimental results of Vardelle and coworkers (Ref 3, 29).

As the molten particles come in contact with the substrate, they lose momentum and spread into flat patches (splats), simultaneously transferring heat to the substrate, which leads to the eventual solidification of the particulates. The local cooling rate of these solidified splats determines the microstructure of the coating. Madejski (Ref 30) has presented a simplified treatment of the solidification of droplets impinging on a cold substrate. This treatment provides an estimate of the final degree of spreading without addressing the transient characteristics accompanying particulate solidification. Trapaga et al. (Ref 31, 32), Moreau et al. (Ref 33), and Watanabe et al. (Ref 34) analyzed the deposition and solidification of a single particle. These studies solved the fluid-flow and heat-transfer equations to determine freezing time, spreading time, final splat diameter, and so on. In a separate study, Gutierrez-Miravete et al (Ref 35) developed a one-dimensional model of the spray deposition process in which molten metallic particles introduced in a carrier gas formed coatings on a substrate. For example, the governing equations for heat transfer between the coatings and the substrate are identical in both cases. In this particular model, layers of molten materials were considered rather than a single molten particle. The rate of deposition of these layers was related to the flow rate/velocity of the particles. Although this deposition process is different from that occurring in the plasma spray process, several similarities exist in the governing equations.

In the present work, one-dimensional models of the torch, spray, and substrate regions were first developed as stand-alone, independent models, based on several currently available analytical and numerical methods that relate the effects of process parameters to the physical phenomena occurring in the three regions. Subsequently, these independent models were coupled into a unified model. To validate the unified model, the spraying of spherical alumina particles in Ar/H_2 and N_2/H_2 plasma was simulated using specific input conditions. This simulation used

Table 1 Typical plasma spray parameters used in the parametric study

Power supply	29 kW
Plasma gas flow rate ($90N_2/10H_2$	100 ft^3/hr
Plasma gas pressure	100 psi
Particle type	Alumina, zirconia, or WC-12Co
Particle diameter	10-80 μm
Carrier gas flow rate (Ar)	37 ft^3/hr
Spray distance	160 mm
Substrate material	Titanium
Nozzle diameter	6 mm
Nozzle length	5 mm
Powder injection point	2 mm from cathode tip

18, 23, 39, and 46 μm diameter alumina particles. The density of the plasma and the velocities and temperatures of the plasma and particles were computed at the torch nozzle exit. These results were then used to obtain the plasma and particle characteristics in the spray region. The simulation results were compared with the experimental data of Vardelle et al. (Ref 3).

Following model validation, a comprehensive parametric study was performed. This study was used to obtain information on the effects of variations in one parameter (e.g., particle type and size on torch, spray, and coating characteristics) while other parameters were kept constant. Table 1 shows the typical plasma spray process parameters used in the parametric study. A N_2/H_2 plasma with alumina, zirconia, or WC-12Co particles ranging in size from 10 to 80 μm were considered in this analysis. These materials were chosen because they exhibit comparatively large differences in density and thermal conductivity values.

4. One-Dimensional Model Description

In addition to those listed earlier, the present one-dimensional model incorporated the following assumptions: steady-state axial flow, constant inner diameter of the torch, velocity of the particles at the injection point equal to carrier gas velocity, metallic particles free from surface oxides, and constant thermophysical particle properties.

4.1 *Torch Region*

Based on these assumptions, the thermodynamic state of a plasma for a given set of input parameters was predicted at the torch nozzle exit by using a one-dimensional compressed flow analysis (Ref 36). Figure 1 shows the control volume used to calculate the initial and final gas density, final velocity, and final temperature at the torch nozzle exit. The particle heating from the point of particle injection in the torch was calculated using a simple one-dimensional numerical scheme with spherical coordinates.

Assuming steady flow, constant nozzle cross-sectional area, and uniform flow at both ends, the equation of mass continuity was derived from:

$$\rho_{in} U_{in} = \rho_{out} U_{out} \qquad \text{(Eq 1)}$$

After simplifying the momentum balance, the velocity of the plasma gas at the nozzle exit was calculated from:

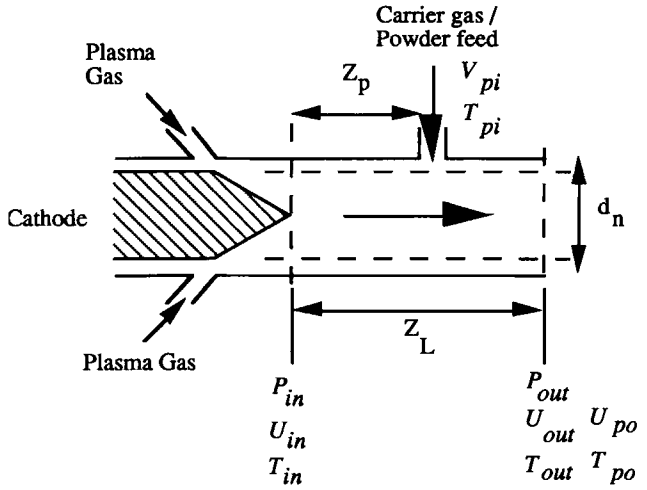

Fig. 1 Control volume used to model the torch region

$$U_{out} = \frac{P_{in} - P_{out}}{\rho_{in} U_{in}} + U_{in} \qquad \text{(Eq 2)}$$

Using conservation of energy, the temperature of the plasma at the nozzle exit was estimated from:

$$T_{out} = T_{in} + \frac{\dot{Q} - \frac{\dot{m}}{2}(U_{out}^2 - U_{in}^2)}{\dot{m} c_p} \qquad \text{(Eq 3)}$$

The heat source term in the above equation included:

$$\dot{Q} = EI - \left(\sum_{i=1}^{n} \dot{m}_c c_{pc} \Delta T_{ci} + \dot{m}_e H_e + \dot{Q}_r \right) \qquad \text{(Eq 4)}$$

where the first term on the right-hand side is the power input, and the second term represents the rate of heat loss due to (1) the coolant flowing through n channels, (2) mass loss of electrode, and (3) radiation. In the present work, an arbitrary arc power efficiency factor of 0.75 was assumed to account for the above heat losses. Relevant inlet and outlet conditions were calculated using the equation of state relating the velocity of sound with mach numbers.

4.2 *Spray Region*

The mathematical model for the spray region was developed to quantitatively determine in-flight characteristics of the coating particle. These characteristics included particle velocity, temperature, size, and fraction of liquid (level of melting). As initial conditions, the model used the calculated values of temperature and velocities of the plasma stream and the coating particles at the torch nozzle exit.

The equations of momentum and heat transfer were solved to calculate the velocity and temperature of the particles traveling in the plasma. Velocity and trajectory of the particle in the plasma are influenced by viscous drag. Assuming spherical particles, the momentum transfer equation was expressed as:

$$\frac{dU_p}{dt} = \frac{3}{4}\frac{C_D}{d_p}\frac{\rho_g}{\rho_p}(U_g - U_p)\,|\,U_g - U_p\,| \qquad \text{(Eq 5)}$$

The drag coefficient, C_D, was expressed in terms of the particle Reynolds number (Ref 13). The Knudsen (noncontinuum) effects on the thermal and momentum transfer between the plasma and the particles were approximated using a correction factor for C_D (Ref 22).

Heating of a spherical particle injected into a plasma jet was described by the following transient heat conduction equation:

$$\rho_p C_p \frac{\partial T}{\partial t} = \frac{1}{r^2}\frac{\partial}{\partial r}\left(r^2 k_p \frac{\partial T}{\partial r}\right) \qquad \text{(Eq 6)}$$

The initial and boundary conditions of the particle were expressed as:

$$T(r,0) = T_\pi \quad r \le \frac{d_p}{2} \qquad \text{(Eq 7)}$$

$$\left(\frac{\partial T}{\partial r}\right)_{r=0} = 0$$

$$\left(k_p \frac{\partial T}{\partial r}\right)_{r=d_p/2} = h(T_g - T_{ps}) \qquad \text{(Eq 8)}$$

The heat-transfer coefficient (h) used to estimate the heat transfer between the plasma and the particle was calculated from the following relationships:

$$h = \frac{\mathrm{Nu}k_g}{d_p} \qquad \text{(Eq 9)}$$

$$\mathrm{Nu} = 2.0 + 0.6\mathrm{Pr}^{0.33}\mathrm{Re}^{0.5} \qquad \text{(Eq 10)}$$

Due to continuous heat transfer from the plasma to the particle, the surface of the particle may reach temperatures greater than the melting point of the particle. To incorporate the effects of phase changes occurring at the melting and boiling points, the latent heats of fusion and vaporization were included in the heat-balance equation through a moving two-phase interface (Ref 27).

Computation of particle temperature and velocity using the above set of equations requires a knowledge of the velocity and temperature profiles of the plasma jet downstream of the torch nozzle exit. Experimental data along with the techniques of curve-fitting were used to obtain empirical relations to describe the variation of plasma velocity and temperature along the axial distance. Although Joshi and Sivakumar (Ref 26) have derived representative equations to describe the variation of plasma velocity and temperature in the spray region and validated them using the experimental data of Vardelle et al. (Ref 3), these equations are relevant to a particular experiment and cannot be directly applied to other plasma spraying conditions. Therefore, in the present work, sufficiently general models were developed for the distribution of plasma temperature and velocity inside and outside the core, using the relationships provided by Scott and Cannell (Ref 18). The core is defined as the length over which the temperature falls linearly with respect to axial distance. The length of the core is calculated following Scott and Cannell's work.

The present model used the following equations to estimate the variation of temperature within and outside the plasma core:

$$T(x) = T(0) - 3.85T(0)x \quad \text{(within the core)} \qquad \text{(Eq 11)}$$

$$T(x) = \left(\frac{1.64\,T(0)}{T(0)}\right)^2\left(\frac{d}{x}\right)(T(0) - T_a) + T_a \quad \text{(outside the core)} \qquad \text{(Eq 12)}$$

where x is the axial distance measured from the torch nozzle exit.

The plasma velocity calculations used a modified version of the Scott and Cannell model (Ref 18), which provided a good fit with the experimental data of Vardelle et al. (Ref 3). This model for plasma jet velocity in the spray was expressed as:

$$U(x) = U(0) \quad 0 \le x \le 4d_n$$

$$U(x) = U(0)\left(\frac{4d_n}{x}\right)^{0.7} \quad x > 4d_n \qquad \text{(Eq 13)}$$

where d_n is the nozzle diameter. The experimental results of Vardelle et al. (Ref 3) were used to validate and modify these models.

4.3 *Substrate Region*

Based on an overall material balance, the instantaneous thickness of the coating was obtained from (Ref 33):

$$X = \left(\frac{\dot{m}_p t}{\rho_p A}\right) \qquad \text{(Eq 14)}$$

Temperature distributions in the coating and the substrate were calculated by solving the following energy equation in one dimension for the variable domain (i.e., substrate and a constantly increasing thickness of spray):

$$\rho\frac{\partial H}{\partial t} = \frac{\partial}{\partial x}\left(k\frac{\partial T}{\partial x}\right) \qquad \text{(Eq 15)}$$

where H represents the overall enthalpy of the system, including the latent heat of fusion liberated during particle solidification. While the flux continuity at the deposit/substrate interface was maintained, the flux at the top surface of the coating (which changes continually) was expressed in terms of heat deposited and heat dissipated into the atmosphere (Ref 33).

4.4 *Void Prediction*

Defects occurring at the boundaries between the substrate and splats and at intersplat boundaries are known to affect the physical characteristics of coatings. In particular, substrate surface roughness plays a significant role in the formation of voids

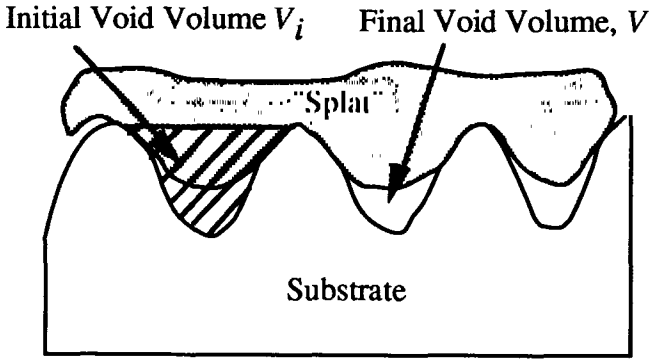

Fig. 2 Schematic diagram illustrating the formation of voids in the valleys between substrate asperity peaks

(porosity) (Ref 37). Considering common surface preparation techniques and spraying conditions that use particle sizes in excess of 20 μm in diameter, the volume of single particles is likely to be larger than the volume enclosed by two adjacent asperity peaks in the surface (Fig. 2). A simple treatment of pore formation is considered in the present model; pores are assumed to result only when the valleys formed by asperity peaks are incompletely filled.

If V_i is the initial volume of the valleys per unit surface area of the substrate, and if the gas contained in this volume is compressed to V after impact by a molten particle ($V << V_i$), then, according to Fukanuma (Ref 37):

$$\left(\frac{V}{V_i}\right)^{1-\Gamma} = \frac{(\Gamma - 1)k_2 \rho_p U^2}{2P_i} \qquad \text{(Eq 16)}$$

where k_2 is a constant and V_i and P_i represent initial volume and pressure, respectively. Equation 16 implies that for a given initial surface condition, the volume of pores in the coating is primarily dependent on particle density and particle velocity. The present model used this relationship to obtain an estimate of the pore volume for a given spraying condition (represented by subscript 1) relative to a standard spraying condition (represented by subscript 2) at constant surface roughness and initial gas pressure:

$$\frac{V_1}{V_2} = \left(\frac{\rho_{p_1} U_1^2}{\rho_{p_2} U_2^2}\right)^{1/(1-\Gamma)} \qquad \text{(Eq 17)}$$

5. Model Validation

5.1 *Torch Region*

In plasma spraying, arc current controls the plasma temperature, with an increase in arc current increasing the plasma temperature. However, the torch nozzle diameter also affects the plasma temperature. Simulations performed using the unified model showed that for a constant plasma gas velocity at the inlet, a progressive decrease in the plasma temperature occurred with an increase in the nozzle diameter (Fig. 3) as a result of faster removal of the heat content from the torch. Also consistent with known observations (Ref 29), a progressive reduction in the difference in temperatures of the plasma generated using three different arc currents occurred with increasing nozzle diameter.

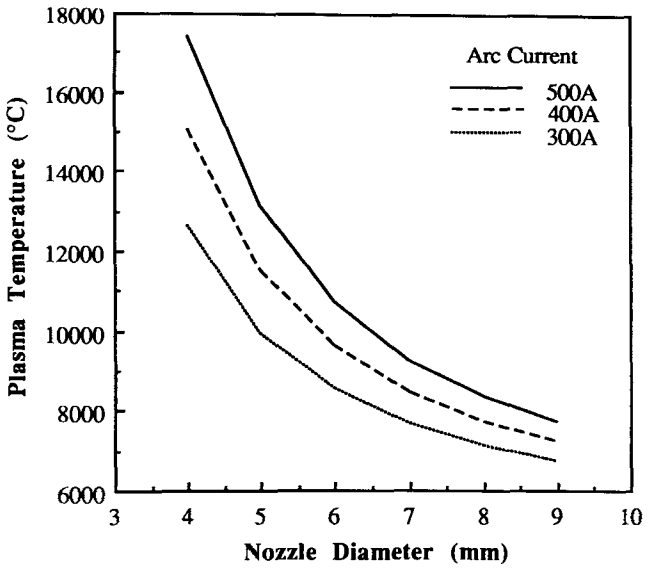

Fig. 3 Computed variation in N_2/H_2 plasma temperature as a function of nozzle diameter, at three levels of arc current

5.2 *Spray Region*

Figures 4(a) and (b) show model predictions of particle velocities for both Ar/H_2 and N_2/H_2 plasma together with the respective experimental data. Both show a reduction in the maximum particle velocity and the final particle velocity (i.e., at the point of striking the surface) with increasing particle size. Comparison of Fig. 4(a) and (b) also shows that, similar to the experimental observations, the model predicts higher particle velocities for the N_2/H_2 plasma than the Ar/H_2 plasma for each particle size. However, unlike the experimental observations, the model results in both cases showed only marginal deceleration of finer particles as they approach the substrate. These differences appear to result from the large number of simplifying assumptions used at each stage of the present unified model. A more rigorous treatment of the particle and plasma dynamics in this region is necessary to minimize these differences.

Figure 5 shows the variations in the surface and core temperatures of 25 and 50 μm diameter zirconia particles sprayed in N_2/H_2 plasma as a function of time. For a given time of flight, the surface and core temperatures of the 25 μm particles were higher than those of the 50 μm particles. These results indicate that control of particle size and use of coarser particles are critical to achieving desirable thermal conditions in the spray, which is in agreement with the literature (Ref 26, 28).

5.5 *Substrate Region*

Figure 6 shows the predicted temperature change of a particle located at the substrate/coating interface as a function of time. Initially, a sharp drop in the temperature of the particle oc-

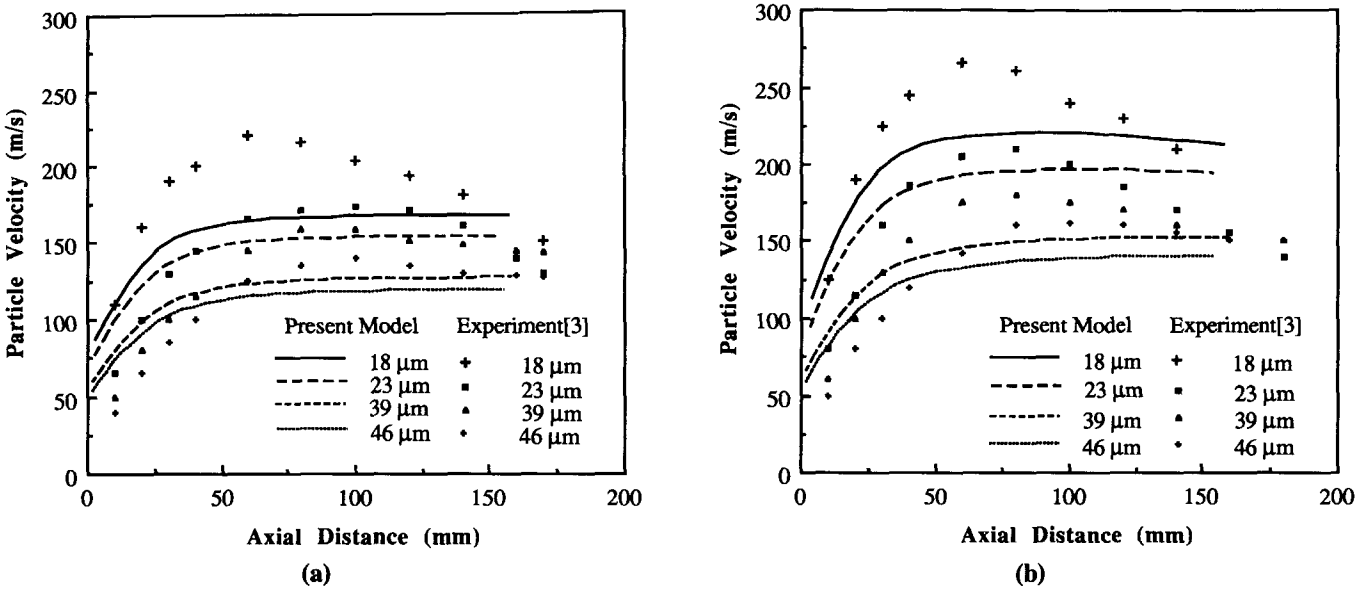

Fig. 4 Comparison of experimental and model predicted velocities of alumina particles in the spray region. (a) Ar/H_2 plasma. (b) N_2/H_2 plasma

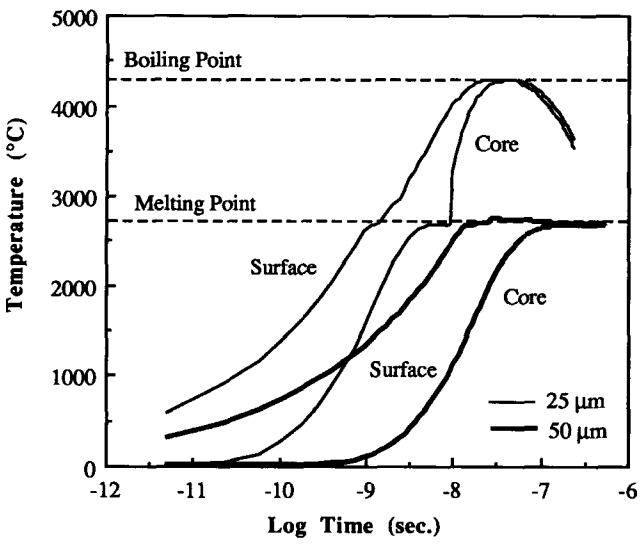

Fig. 5 Computed variations in the temperature of 25 and 50 μm zirconia particles in N_2/H_2 plasma as a function of time

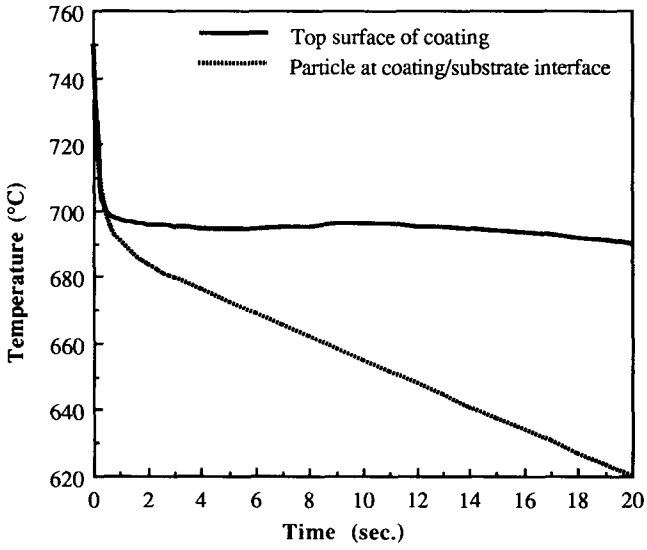

Fig. 6 Computed temperatures of (a) a deposited particle located at the coating/substrate interface and (b) the top surface of the coating as the coating builds up

curs from the quenching action of the substrate. Also shown is the predicted variation of the temperature of the top surface of the coating as the coating builds up over time. The temperature of the coating drops rapidly when the first layer is deposited and gradually decreases as additional layers are deposited over the initial layer. Figure 7 shows the increase in the temperature of a point in the substrate located 1 mm below the substrate/coating interface due to the deposition of the particle. The temperature of this point increases rapidly during the initial stages, subsequently levels off, and later begins to decrease with time. These temperature predictions were consistent with work reported by Gutierrez-Miravete et al. (Ref 35).

6. Parametric Study

6.1 *Torch Region*

The particle velocity at the torch nozzle exit depends on process parameters and feedstock material characteristics. Figure 8 shows the effect of particle diameter on the velocity of zirconia particles at the torch nozzle exit. Particle velocity is influenced by the distance of the point of injection of the carrier gas from the cathode (Z_p). Although carrier gas injection outside the torch nozzle exit is common practice, Fig. 8 shows that higher particle

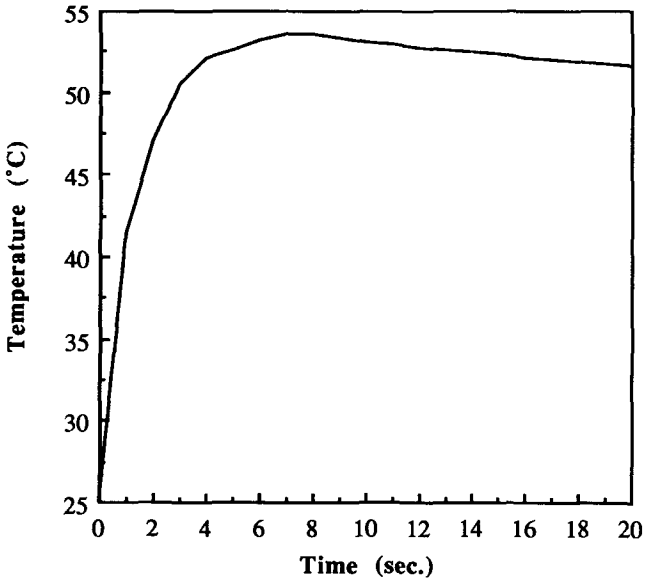

Fig. 7 Computed heating of the substrate at a location 1 mm below the coating/substrate interface

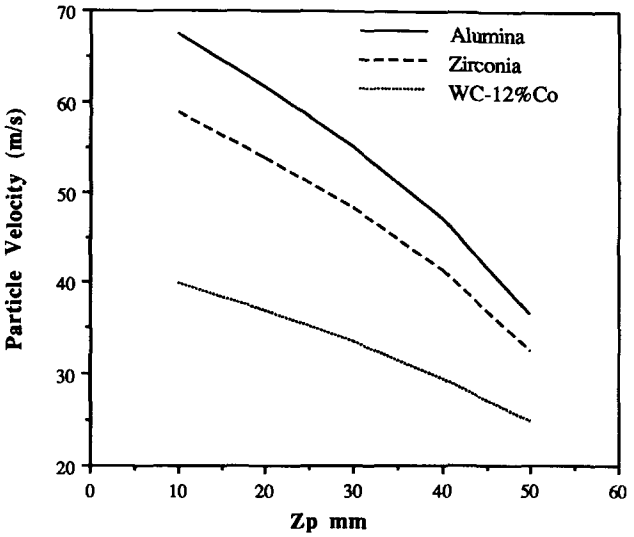

Fig. 9 Computed particle velocity at the torch nozzle exit as a function of the distance between the carrier gas (particle) injection point and the cathode tip for three different types of materials in N_2/H_2 plasma. Particle size, 20 μm

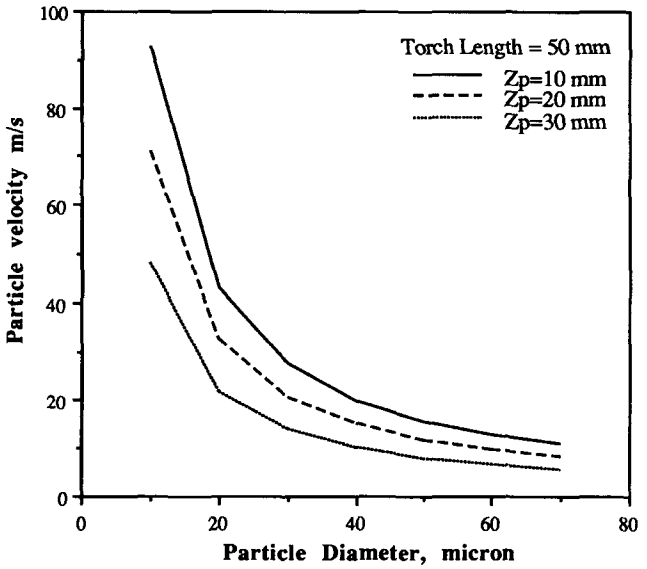

Fig. 8 Computed variation of zirconia particle velocity at the torch nozzle exit as a function of particle diameter in N_2/H_2 plasma, for three different positions of the carrier gas (particle) injection point from the cathode

velocities are obtained with longer travel distance of the particles inside the torch. However, larger particles (greater than 40 μm diameter), which accelerate slowly, show only marginal differences in torch exit velocities.

Figure 9 highlights the effects of Z_p on the velocity of three different types of particles. For a given Z_p, the lighter alumina particles show a rapid acceleration compared to the heavier WC-12Co and zirconia particles. These results indicate that it is preferable to inject coarse, high-density particles inside the torch to attain higher particle velocities, whereas injection of fine, low-density particles outside the torch nozzle exit may not adversely affect the final particle velocity at the substrate. In fact, this practice will eliminate the occurrence of "choking" when fine particles are injected within the torch nozzle.

Particle temperature can be controlled by varying the arc current. For a given zirconia particle diameter, as shown in Fig. 10, the particle temperature increases steadily with arc current until the solidus temperature is reached, after which the rate of temperature increase suddenly decreases due to phase change. It is evident that, for ceramic powders such as zirconia, sufficient softening of particles can be accomplished at current levels in the range of 400 to 500 A. If the particles impinge on the substrate in a softened state with high velocities, it may be possible to obtain sound coatings (Ref 38), the rationale being that partially molten or softened particles produce minimal voids and minimize residual stresses more than completely melted or superheated particles.

6.2 *Spray Region*

Particles exiting from the torch are further accelerated and heated by the plasma jet in the spray region. The velocity and temperature at which particles strike the substrate are crucial factors in final coating quality. Figure 11 shows a comparison of velocities of zirconia and WC-12Co particles of the same size as they travel in the spray. The WC-12Co particles are approximately two and a half times heavier than the zirconia particles and thus do not accelerate to the same extent as the zirconia particles.

In the spray region, particle size also plays an important role in determining the coating quality. It is clear from Fig. 12 that particles finer than 25 μm in diameter attain very high temperatures (close to the boiling point) when they reach the substrate, leading to mass loss due to evaporation. In contrast, particles larger than 80 μm may not reach a temperature sufficiently high to spread when they strike the substrate. This analysis indicates that 50 to 65 μm particles would soften and spread since they are close to the melting point.

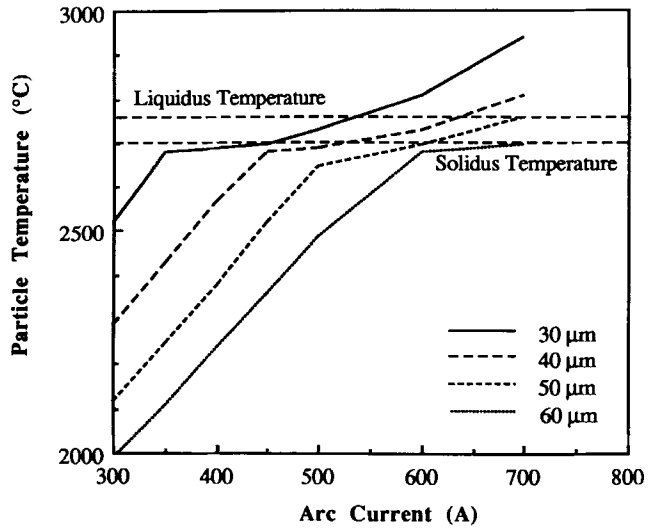

Fig. 10 Computed surface temperatures of zirconia particles at the torch nozzle exit as a function of arc current in N_2/H_2 plasma

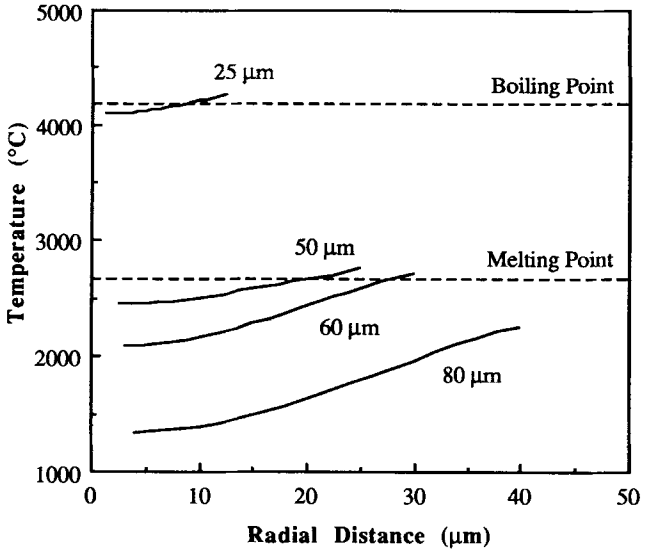

Fig. 12 Computed temperature distribution in zirconia particles of various diameters in a N_2/H_2 plasma jet for a spray distance of 40 mm

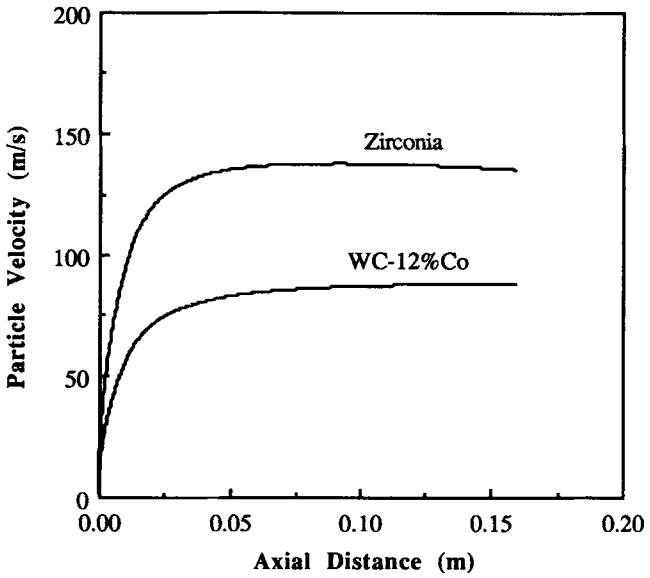

Fig. 11 Computed velocity of 50 μm diameter particles in a N_2/H_2 plasma stream

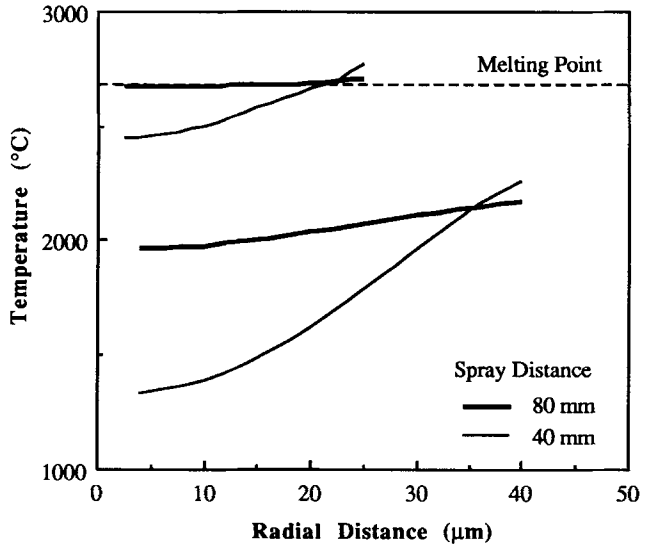

Fig. 13 Effect of spray distance on the computed temperature of zirconia particles as a function of particle size

Figure 13 shows the effects of spray distance and particle size on particle temperature distribution for plasma spraying of zirconia particles. At a 40 mm spray distance, a substantial temperature gradient is observed across the radius of the particles. In contrast, the particle temperature profile is flatter at an 80 mm spray distance, which appeared to result from the longer residence time of the particle in the spray. In fact, at an 80 mm spray distance, the 50 μm diameter particles appear to undergo complete melting.

6.3 *Substrate Region*

Table 2 shows a relative estimate of porosity as a function of particle size and type. For the sake of convenience, the void volume for plasma spraying 10 μm particles was used as a reference. Table 2 indicates that on a relative scale, larger particles would result in a higher porosity than smaller particles. In the present analysis, this behavior is attributed to lower particle velocity of larger-size particles compared to fine particles. For the same reason, the WC-12Co particles show higher levels of porosity than the zirconia particles for heavier (denser) coating materials, use of fine powder particles is likely to reduce the void content in the resultant coating.

The results of this parametric study indicate that the unified one-dimensional model for the plasma spray process will enable evaluation of effects of a given set of input process parameters and the selection of an optimal set of parameters. A statistical design of experiments based on this optimal set of parameters

Table 2 Estimates of void volume obtained with different particle sizes

Particle diameter, μm	Relative void volume	
	Zirconia	WC-12Co
25	1.24	1.42
50	1.59	1.88
60	1.71	2.01
80	1.92	2.27

would complement the model predictions and thereby enable the user to select an operational window for producing high-quality plasma spray coatings.

7. Summary

A simple, unified, one-dimensional plasma spray process model has been developed to relate the effects of plasma spray parameters on the thermokinetic properties of the plasma and particles and on the void content. A parametric analysis of the model indicated that plasma gas type, arc current, location of particle injection port, particle type, and particle size affect the final temperature and velocity of the particles. An analysis based on the model results will enable a user to select and optimize plasma spray process parameters in order to obtain high-integrity coatings. The structure of the current unified one-dimensional plasma spray process model is modular in nature and is suitable for addressing other spraying processes (e.g., the high-velocity oxyfuel process).

Acknowledgment

This work was conducted by the National Center for Excellence in Metalworking Technology (NCEMT), operated by Concurrent Technologies Corporation, under contract to the U.S. Navy as a part of the U.S. Navy Manufacturing Technology (ManTech) Program.

References

1. D.A. Gerdeman and N.L. Hecht, *Arc Plasma Technology in Materials Science*, Springer-Verlag/Wien, 1972
2. D.R. Mash, N.E. Weare, and D.L. Walker, Process Variables in Plasma-Jet Spraying, *J. Met.*, Vol 13 (No. 7), 1961, p 473-478
3. M. Vardelle, A. Vardelle, P. Fauchais, and M.I. Boulos, Plasma-Particle Momentum and Heat Transfer: Modelling and Measurements, *AIChE J.*, Vol 29 (No. 2), 1983, p 236-243
4. E. Lugscheider, I. Rass, H.L. Heijnen, P. Chandler, T. Cosak, P. Fauchais, A. Denoirjean, and A. Vardelle, Comparison of the Coatings Properties of Different Types of Powder Morphologies, *Thermal Spray: International Advances in Coatings Technology*, C.C. Berndt, Ed., ASM International, 1992, p 967-973
5. E. Pfender, Plasma Generation by Arcs—An Overview, *Thermal Plasma Applications in Materials and Metallurgical Processing*, N. El-Kaddah, Ed., TMS, 1992, p 13-30
6. D. Apelian, A New Horizon for Plasma Processing, *Thermal Plasma Applications in Materials and Metallurgical Processing*, N. El-Kaddah, Ed., TMS, 1992, p 3-12
7. J. Szekely and R.C. Westhoff, Recent Advances in the Mathematical Modeling of Transport Phenomena in Plasma Systems, *Thermal Plasma Applications in Materials and Metallurgical Processing*, N. El-Kaddah, Ed., TMS 1992, p 55-74
8. M.I. Boulos, RF Induction Plasma Spraying: State-of-the-Art Review, *J. Thermal Spray Technol.*, Vol 1 (No. 1), 1992, p 33-40
9. H.A. Stine and V.R. Watson, "The Theoretical Enthalpy Distribution of Air in Steady Flow along the Axis of a Direct Current Electric Arc," TN D-1331, National Aeronautics and Space Administration, 1962
10. V.R. Watson and E.B. Pegot, "Numerical Calculations for the Characteristics of a Gas Flowing Axially through a Constricted Arc," TN D-4042, National Aeronautics and Space Administration, 1962
11. A. Mazza, "Studies of an Arc Plasma Reactor for Thermal Plasma Synthesis," Ph.D. dissertation, University of Minnesota, 1983
12. A.H. Dilwari and J. Szekely, Fluid Flow and Heat Transfer in Plasma Reactors. I. Calculation of Velocities, Temperature Profiles and Mixing, *J. Heat Mass Transfer*, Vol 30 (No. 11), 1987, p 2357-2372
13. D.A. Scott, P. Kovita, and G.N. Haddah, Temperature in the Plume of a DC Plasma Torch, *J. Appl. Phys.*, Vol 66 (No. 11), 1989, p 5232-5239
14. R.A. Neiser, R.C. Dykhuizen, M.F. Smith, and K.J. Holls, Use of Computer Model to Assist in VPS Parameter Development, *Thermal Spray Coatings: Research, Design and Applications*, C.C. Berndt and T.F. Bernecki, Ed., ASM International, 1993, p 61-66
15. D. Apelian, M. Paliwal, R.W. Smith, and W.F. Schilling, Melting and Solidification in Plasma Spray Deposition—Phenomenological Review, *Int. Met. Rev.*, Vol 28 (No. 5), 1983, p 271-294
16. J.M. Houben, Future Developments in Thermal Spraying, *Proc. 9th Int. Thermal Spray Conf.*, ASM International, 1980, p 143-154
17. S.V. Joshi, Plasma Spraying of WC-Co. Part I: Theoretical Investigation of Particle Heating and Acceleration During Spraying, *J. Thermal Spray Technol.*, Vol 2 (No. 2), 1993, p 127-132
18. B.F. Scott and J.K. Cannell, Arc Plasma Spraying—An Analysis, *Int. J. Machine Tool Design Res.*, Vol 7, 1967, p 243-256
19. R. Westhoff, G. Trapaga, and J. Szekely, Plasma Particle Interactions in Plasma Spraying Systems, *Metall. Trans. B*, Vol 23B, 1992, p 683-693
20. A.H. Dilwari, J. Szekely, J. Batdorf, R. Detering, and C.B. Shaw, The Temperature Profiles in an Argon Plasma Issuing into Atmosphere: A Comparison of Measurements and Predictions, *Plasma Chem. Plasma Proc.*, Vol 10 (No. 2), 1990, p 321-336
21. D.J. Varacalle, Jr., R.L. Miller, J.A. Walter, and G. Irons, Analytically Modeling the Plasma Spraying of Nickel-Aluminum Powder, *Heat Transfer in Thermal Plasma Processing*, HTD—Vol 161, American Society of Mechanical Engineers, 1991, p 137-143
22. X. Chen and E. Pfender, Effect of the Knudsen Number on Heat Transfer to a Particle Immersed into a Thermal Plasma, *Plasma Chem. Plasma Proc.*, Vol 3 (No. 1), 1983, p 97-113
23. R. Spores and E. Pfender, Flow Structure of a Turbulent Thermal Plasma Jet, *Surf. Coat. Technol.*, Vol 37, 1989, p 251-260
24. K.G. Shaw and R.M. German, Determination of the Proper Particle and Size Distribution Required for Plasma Spraying and Atomization, *Advances in Powder Metallurgy—1991*, Vol 5, P/M Materials, 1991, p 263-275
25. P. Fauchais, A. Vardelle, and M. Vardelle, Modelling of Plasma Spraying of Ceramic Coatings at Atmospheric Pressure, *Ceram. Int.*, Vol 17, 1991, p 367-378
26. S.V. Joshi and R. Sivakumar, Prediction of In-flight Particle Parameters during Plasma Spraying of Ceramic Powders, *Mater. Sci. Technol.*, Vol 8, 1992, p 481-488
27. D.K. Das and R. Sivakumar, Modelling of the Temperature and the Velocity of Ceramic Powder Particles in a Plasma Flame—I. Alumina, *Acta Metall. Mater.*, Vol 38 (No. 11), 1990, p 2187-2192
28. D.K. Das and R. Sivakumar, Modelling of the Temperature and the Velocity of Ceramic Powder Particles in a Plasma Flame—II. Zirconia, *Acta Metall. Mater.*, Vol 38 (No. 11), 1990, p 2193-2198
29. M. Vardelle, A. Vardelle, and P. Fauchais, Spray Parameter and Particle Behavior Relationships during Plasma Spraying, *J. Thermal Spray Technol.*, Vol 2 (No. 1), 1993, p 79-91

30. J. Madejski, Solidification of Droplets on a Cold Surface, *Int. J. Heat Mass Transfer*, Vol 19, 1976, p 1009-1013
31. G. Trapaga and J. Szekely, Mathematical Modeling of the Isothermal Impingement of Liquid Droplets in Spraying Processes, *Metall. Trans. B*, Vol 22B, 1991, p 901-914
32. G. Trapaga, E.F. Matthys, J.J. Valencia, and J. Szekely, Fluid Flow, Heat Transfer, and Solidification of Molten Metal Droplets Impinging on Substrates: Comparison of Numerical and Experimental Results, *Metall. Trans. B*, Vol 23B, 1992, p 701-718
33. C. Moreau, P. Cielo, and M. Lamontagne, Flattening and Solidification of Thermally Sprayed Particles, *J. Thermal Spray Technol.*, Vol 1 (No. 14), 1992, p 317-323
34. T. Watanabe, I. Kuribayashi, T. Honda, and A. Kanzawa, Deformation and Solidification of a Droplet on a Cold Substrate, *Chem. Eng. Sci.*, Vol 47 (No. 12), 1992, p 3059-3065
35. E. Gutierrez-Miravete, E.J. Lavernia, G.M. Trapaga, J. Szekely, and N.J. Grant, A Mathematical Model of the Spray Deposition Process, *Metall. Trans. A*, Vol 20A, 1989, p 71-85
36. A.H. Shapiro, *Compressible Fluid Flow*, Vol 1, Ronald Press, 1953
37. H. Fukanuma, in *Thermal Spray: International Advances in Coatings Technology*, C.C. Berndt, Ed., ASM International, 1992, p 767-772
38. L.S. Sokol, C.C. McComas, and E.M. Hanna, Plasma Spray Method and Apparatus, U.S. Patent 4,256,779, March 1981